Proceedings of 2009 ASME International Mechanical Engineering Congress & Exposition
IMECE2009
November 13-19, Lake Buena Vista, Florida

IMECE2009-12651

IMPROVING THE PERFORMANCE OF A THERMAL COMPRESSOR IN A STEAM EVAPORATOR VIA CFD ANALYSIS

Xianchang Li
Department of Mechanical Engineering
Lamar University
Beaumont, TX 77710

Ting Wang and Benjamin Day
Energy Conversion and Conservation Center
University of New Orleans
New Orleans, LA 70148

ABSTRACT

Ejectors have been widely used in many applications such as water desalination, steam turbine power generation, refrigeration systems, and chemical plants. The advantage of an ejector system lies in its extremely reliable and stable operation due to the complete absence of moving parts. However, the performance depends on a number of factors, among which the flow channel configuration/arrangement is very critical. A comprehensive study mainly focusing on the sensitivity of performance on the geometric arrangement was conducted in this paper to improve an existing thermal compressor performance in a steam evaporator. The performance is measured by the suction (secondary) flow rate of the primary steam jet from a low-pressure vapor plenum. Numerical simulation is employed to investigate the thermal-flow behavior. It is observed that any downstream resistance will seriously impede the suction flow rate. In addition, the suction rate is found to be sensitive to the location of the jet exit, and there is an optimum location where the jet should be issued. A well-contoured diffuser can increase the suction rate significantly. However, the size of suction opening to the plenum is less important, and a contoured annular passage to guide the entrained flow shows little effect on the overall performance. Based on the numerical results the steam suction rate of the best case in the confinement of the current study is approximately 430% the jet flow rate, while some cases with mediocre design can only produce an entrainment of 24% the jet flow.

Keywords: Ejector, thermal compressor, performance simulation

NOMENCLATURE

c_p	specific heat (J/kg-K)
D	ejector pipe diameter (m)
d	diameter of steam jet or contraction cones (m)
k	turbulence kinetic energy (m^2/s^2)
h	convective heat transfer coefficient (W/m^2-K)
L, l	length (m)
$\dot{m}$	mass flow rate (kg/s)
P	pressure (N/m^2)
Pr	Prandtl number, ν/α
Re	Reynolds number, ud/ν
T	temperature (K, ^oF)
u	streamwise velocity component (m/s)
u', T'	turbulence fluctuation terms
v	radial velocity component (m/s)
x, y	coordinates

Greek

α	thermal diffusivity (m^2/s)
ε	turbulence dissipation rate (m^2/s^3)
η	suction rate, $\dot{m}_s / \dot{m}_j$
λ	heat conductivity (W/m-K)
μ	dynamic viscosity (kg/m-s)
ν	kinematic viscosity (m^2/s)
ρ	density (kg/m^3)
τ	stress tensor ($kg/m\text{-}s^2$)

Subscript

j	jet
s	secondary flow
t	turbulent

1. INTRODUCTION

An ejector generally utilizes the momentum of a high-velocity primary jet of vapor to entrain and accelerate a medium in still or moving in a low speed. The functions of an ejector include maintaining vacuum in evaporation, removing air from condensers as a vacuum pump, augmenting thrust, or increasing vapor pressure as a thermal compressor. The thermal compressor is an ejector, but it further utilizes the thermal energy to augment the performance by reducing the size of a conventional multi-stage evaporator. Ejectors have been widely applied in water desalination plants, steam turbines, geothermal power plants, refrigeration systems, and chemical plants. The application of ejectors in these fields has a long history. For example, for many years, steam jet ejectors have been the driving force to produce vacuum in the chemical process industries. Power [1] systematically documented the working mechanism of ejector stages and discussed the engineering calculations. A review was also given in [1] to steam-jet refrigeration, steam-jet and gas-jet compressors, liquid jet eductors, and desuperheaters.

As the pressure for high energy efficiency increases, a number of studies have been conducted to improve the performance of an ejector or a system with ejectors. The aero-thermal performance of an ejector can be defined as the vacuum maintained or the amount of medium removed through a certain high-pressure flow. The ejector performance depends on a number of factors, and the flow channel design/arrangement is very critical. For example, Balamurugan et al. [2] performed detailed experiments as well as numerical simulation to understand the hydrodynamic characteristics of the ejector geometry. It was shown that there is an optimum ratio of nozzle area to throat area (area ratio) at which the liquid entrainment rate is the highest. For a wide variety of ejector geometries and operating conditions, the liquid entrainment rate correlates with the pressure difference between the water surface in the suction chamber and the throat exit.

For a steam-ejector refrigeration system, Chen and Sun [3] experimentally investigated the controlling parameters of a steam ejector, including operating conditions and the exit Mach number of the primary nozzle. Operation maps were constructed to help the design of steam-ejectors and from the experimental results the empirical equations were correspondingly derived. It was reported that an excessively high Mach number at the primary nozzle exit is not necessary, and a moderate value should be 4.35. Rusly et al. [4] modeled several ejector designs using finite volume CFD techniques to resolve the flow dynamics in the ejectors. Flow conditions resulting from ejector geometry variations were discussed. It was found that the maximum entrainment ratio happens in the ejector just before a shock occurs and the position of the nozzle is an important ejector design parameter. Pianthong et al. [5] predicted numerically the flow phenomena and performance of two types of steam ejectors used in a refrigeration system. They concluded that the computational fluid dynamics (CFD) can predict ejector performance very well and revealed the effect of operating conditions on an effective area is directly related to its performance. In addition, it was found that the flow pattern does not depend much on the suction zone. Riffat and Everitt [6] designed a steam jet ejector for air conditioning in a small motor vehicle. The coolant and/or exhaust heat from the engine was used to drive the ejector cycle. Experimental tests and numerical simulation were used to validate the design and determine the performance.

Research has also been conducted for application of ejectors in desalination. Ji et al. [7] established a simulation model of steam ejectors used in a thermal vapor compression desalination system. The performance under different operating conditions was then calculated. The results indicated that entrainment ratio decreased with increasing compression pressure when the compression pressure exceeded design value, and the entrainment ratio maintained at a constant value when compression vapor pressure was lower than the design value. A motive steam pressure either lower or higher than the design point could result in bad performance. Elkady et al. [8] presented an experimental investigation of the performance of the ejector used in desalination applications with air as the working fluid. The effect of the operating conditions, ejector geometry, and the relative position of the primary nozzle exit within the mixing chamber on the ejector performance was studied. The results showed that using a convergent-divergent nozzle enhances the performance of the ejector. The entrainment ratio increases with increasing primary pressure, and the entrained flow reaches a maximum at a certain primary pressure. Recently, Negeed [9] investigated the performance of the ejector by using numerical simulation (CFD). The ejector is for desalination applications and the working fluid is air. The effect of operating conditions and ejector geometry on ejector performance was examined. The results showed that ejector performance increases by increasing the primary nozzle throat diameter, and the entrained flow reaches a maximum at a certain diameter. The optimum position with respect to the ejector's mixing chamber and the mixing length were determined.

Discussion on fundamental flow field and control of an ejector is also seen in the public domain. Kim et al. [10] conducted a numerical study on the flow characteristics inside a variable ejector. The variable ejector is used to obtain a specific recirculation ratio under a given operating pressure ratio by varying the ejector throat area ratio. The sonic and supersonic nozzles were adopted as primary driving nozzles, and a movable cone cylinder, inserted into a conventional ejector-diffuser system, was used to change the ejector throat area ratio. Kim et al. [11] investigated the influence of various geometric parameters and pressure ratios on the Coanda ejector performance. In Coanda ejectors, the secondary flow is dragged into the ejector, following a curved contour without separation, due to the primary flow momentum. The effect of various factors, such as the pressure ratio, primary nozzle and ejector configurations on the system performance was examined. It was found that the performance of the Coanda ejector strongly depends on the primary nozzle configuration and the pressure ratio. The mixing layer growth plays a major role in optimizing the performance of the Coanda ejector as it

decides the ratio of secondary mass flow rate to primary mass flow rate and the mixing length. Sriveerakul et al. [12] studied the flow mixing process of a steam ejector used in a jet refrigeration cycle by using the software package (FLUENT). The flow structure of the modeled ejectors was analyzed when its operating conditions and geometries were varied.

A comprehensive study was conducted in this study to improve the performance of an existing thermal compressor in a steam evaporator. The system is designed to distill brine water effectively with a 2-effect evaporator. Traditionally, the multiple-stage thermal compressors that apply the vacuum suction principle (Bernoulli's principle) can be used to increase the steam flow exchange rate via a series of steam jets. The 2-effect evaporator is to reduce the conventional system's size from eight stages to two stages with a similar capital cost. The designed output is 160 gallons/min (0.01 m^3/s) by using a steam flow of 10,000 lbm/hr at 45 psig. However, after installation the actual output was only 47-60 gallon/min, which is significantly lower than the designed value. Tthis study is to employ CFD simulation to investigate the thermal-flow behavior and the reason of failure and to provide an improved design to achieve the best performance under the current space constraint. The performance is measured by the suction (secondary) flow rate of the primary steam jet from a low-pressure vapor plenum. More specifically, the effects of the jet exit location, diffuser contour, suction opening size, and downstream resistance on the ejector suction flow rate are explored.

2. GOVERNING EQUATIONS AND NUMERICAL METHOD

The time-averaged steady-state Navier-Stokes equations as well as the equations for mass and energy for compressible flows need to be solved, and the equations are given as follows.

$$\frac{\partial}{\partial x_i}\left(\rho u_i\right)=0 \tag{1}$$

$$\frac{\partial}{\partial x_i}\left(\rho u_i u_j\right)=\rho \bar{g}_j-\frac{\partial P}{\partial x_j}+\frac{\partial}{\partial x_i}\left(\tau_{ij}-\rho\overline{u'_i u'_j}\right) \tag{2}$$

$$\frac{\partial}{\partial x_i}\left(\rho c_p u_i T\right)=\frac{\partial}{\partial x_i}\left(\lambda\frac{\partial T}{\partial x_i}-\rho c_p\overline{u'_i T'}\right)+\mu\Phi \tag{3}$$

where τ_{ij} is the symmetric stress tensor defined as

$$\tau_{ij}=\mu\left(\frac{\partial u_j}{\partial x_i}+\frac{\partial u_i}{\partial x_j}-\frac{2}{3}\delta_{ij}\frac{\partial u_k}{\partial x_k}\right). \tag{4}$$

$\mu\Phi$ is the viscous dissipation and λ is the heat conductivity. The terms of $\rho\overline{u'_i u'_j}$ and $\rho c_p\overline{u'_i T'}$ represent the Reynolds stresses and turbulent heat fluxes, respectively. These two terms need be modeled properly for a turbulent flow.

Turbulence Model

A widely applied group of turbulence models are the k-ε model, which, based on the Boussinesq hypothesis, relates the Reynolds stresses to the mean velocity as

$$-\rho\overline{u'_i u'_j}=\mu_t\left(\frac{\partial u_i}{\partial x_j}+\frac{\partial u_j}{\partial x_i}-\frac{2}{3}\delta_{ij}\frac{\partial u_k}{\partial x_k}\right)-\frac{2}{3}\rho k\delta_{ij} \tag{5}$$

where k is the turbulent kinetic energy and μ_t is the turbulent viscosity. Correspondingly, the turbulent heat fluxes can be modeled with the turbulent heat conductivity (λ_t) as given by

$$\rho c_p\overline{u'_i T'}=-\lambda_t\frac{\partial T}{\partial x_i}=-c_p\frac{\mu_t}{Pr_t}\frac{\partial T}{\partial x_i}, \tag{6}$$

where Pr_t is the turbulence Prandtl number. The standard k-ε model is mainly valid for fully-turbulent flows with high Reynolds number. To simulate flows with both highly turbulent and low velocity laminar zones, the RNG-based k-ε model is a better option [13]. The RNG k-ε model was derived using a renormalization group theory, a statistical technique, although the equations are in the similar form to the standard k-ε model. However, the RNG theory provides an analytically-derived differential formula for the effective viscosity that accounts for low-Reynolds-number effects, and an analytical formula for turbulent Prandtl numbers. The equations for the turbulent kinetic energy (k) and the dissipation rate (ε) are:

$$\frac{\partial}{\partial x_i}\left(\rho u_i k\right)=\frac{\partial}{\partial x_i}\left[\alpha_k\mu_{eff}\frac{\partial k}{\partial x_i}\right]+G_k-\rho\varepsilon+Y_M. \tag{7}$$

$$\frac{\partial}{\partial x_i}\left(\rho u_i \varepsilon\right)=\frac{\partial}{\partial x_i}\left[\alpha_\varepsilon\mu_{eff}\frac{\partial \varepsilon}{\partial x_i}\right]+C_{1\varepsilon}G_k\frac{\varepsilon}{k}-C_{2\varepsilon}\rho\frac{\varepsilon^2}{k}-R_\varepsilon. \tag{8}$$

The term G_k is the generation of turbulence kinetic energy due to the mean velocity gradients, and Y_M represents the contribution of the fluctuating dilatation in compressible turbulence to the overall dissipation rate. α_k and α_ε are the inverse effective Prandtl numbers for k and ε, respectively. R_ε in the ε equation is an additional term to the standard k-ε model. This term is designed to significantly improve the accuracy for rapidly strained flows. Note the k and ε equations in a general format may include more terms to take into account the effect of buoyant effect as well as extra sources. For high-Reynolds-number flows, the formula for turbulent viscosity is reduced to

$$\mu_t=\rho C_\mu k^2/\varepsilon \tag{9}$$

where the constant C_μ is 0.845, while this constant is 0.09 for the standard k-ε model. The constants $C_{1\varepsilon}$ and $C_{2\varepsilon}$ in the RNG model are 1.42 and 1.68, respectively.

Enhanced Wall Function

Effective use of the RNG model depends on an appropriate treatment of the near-wall region. Special treatment is needed in the region close to the wall. The enhanced wall function is one of the methods that model the near-wall flow. In the enhanced wall treatment, the two-layer model is combined with the wall functions. The whole domain is separated into a viscosity-affected region and a fully turbulent region by defining a turbulent Reynolds number, Re_y,

$$Re_y=yk^{1/2}/\nu \tag{10}$$

where k is the turbulence kinetic energy and y is the distance from the wall. The two-equation k-ε model is used in the fully turbulent region where $Re_y > 200$, and the one-equation model of Wolfstein [14] is used in the viscosity-affected region with $Re_y < 200$. The turbulent viscosities calculated from these two regions are blended with a blending function (θ) to smoothen the transition.

$$\mu_{t,enhanced} = \theta\mu_t + (1-\theta)\mu_{t,l} \quad (11)$$

where μ_t is the viscosity from the k-ε model, and $\mu_{t,l}$ is the viscosity from the near-wall one-equation model. The blending function is defined so that it is equal to 0 at the wall and 1 in the fully turbulent region. The linear (laminar) and logarithmic (turbulent) laws of the wall are also blended to make the wall functions applicable throughout the entire near-wall region. The similar approach to the near-wall temperature distribution is also employed. More details can be seen in [15].

Numerical Method

The commercial software package Fluent (version 6.3.26) is used in this study. The governing equations are discretized by the finite volume method, and the second order upwind scheme is adopted for spatial discretization of the convection terms [15]. The segregated solver is used in the simulation, and the SIMPLE algorithm (Patankar [16]) is employed to couple the pressure and velocity. The convergence criteria of iterative solution have been insured when the residual of all variables are less than specific values. The value is 10^{-4} for continuity and momentum, and 10^{-6} for energy.

3. GEOMETRY AND BOUNDARY CONDITIONS

As documented in the later part of this paper, the existing design is first analyzed, followed by different modifications on the geometric configuration to reveal the sensitivity of the performance to different flow channel arrangements. Based on analysis of the field data via estimated energy and mass balances, the suction flow rate is very low -- only about 24% of the designed value, which should be about 3.5 times of the jet flow rate. The simplified geometry of the existing design is shown in Figure 1(a). It was assumed the flow is axisymmetric. The total length of the pipe is L=6.30 m (248 inches) with a diameter of D=0.508 m (20 inches). The diameter of the jet is d=0.0508 m (2 inches), injecting from the same location as the contraction cone entrance in the mainstream direction. The first contraction cone is close to the steam jet and has a length of l_1=0.559 m (22 inches). The other two downstream contraction cones have a length of 0.533 m (21 inches) each (l_2=l_3). The exit diameters of the three contraction cones (d_1, d_2, and d_3) are 0.127, 0.112, and 0.102 m (or 5.0, 4.4 and 4.0 inches), respectively. The left cone is located at L_1=0.711 m (28 inches) from the left end of the pipe. The distance between the other two cones is 0.508m (20 inches) (L_2). Starting from the left end, the suction opening is 0.610 m (24 inches) (L_3).

Figure 1 (b) shows the geometric scheme of the best case by combining all the favorable features, a contoured contraction cone with a long diffuser added downstream (66 inches or 1.68 m) and a transition piece (4 inches or 0.1 m) between the contraction and the diffuser. The diffuser has a diffusion angle of 6.5°. There is no contraction cone downstream.

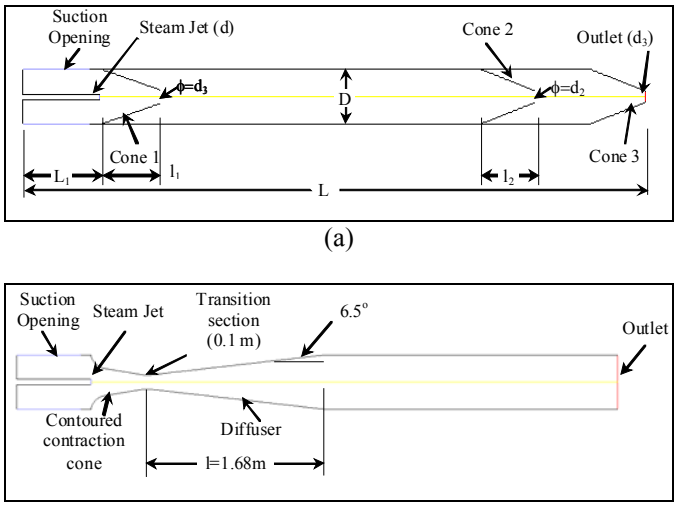

Figure 1: Geometric scheme of (a) the existing design and (b) the case with best performance

For numerical analysis, the suction opening and the outlet are at a constant pressure (atmosphere). The jet velocity is 100 m/s with a total flow rate of 0.099 kg/s. The steam jet is assumed to be at 450 K (350 °F), and the suction flow has a temperature of 373K (212 °F). These parameters give a jet Reynolds number (Re) of 135,556, which means the flow is turbulent. Heat transfer between the jet and suction flow is calculated, and the compressibility effect is also considered. Notice that in the real situation the jet mass flow rate is higher due to its higher pressure. It is believed that the mechanism of suction presented in this study can be applied to the real system with higher pressures. Because the critical factor is the pressure difference, the actual pressure plays a secondary role.

4. MESHING AND GRID INDEPENDENCE STUDY

The characteristics of baseline case meshing are shown in Fig. 2. The non-uniform unstructured mesh is employed in the whole domain. There are more cells close to the regions with large velocity or pressure gradients. The total number of cells in this study is about 11,184. Grid independence is examined for all the cases, and one of the examples is shown in Table 1. It is observed that when the cell number increases to 44,736, the exit mass flow rate and the maximum pressure change only by less than 1.0%. Therefore, it can be proven that the overall performance is not affected by the grid and the results are independent of the employed mesh numbers.

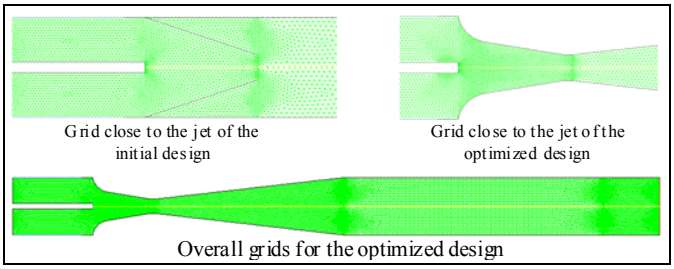

Figure 2: Computational meshes for different cases

Table 1: Overall performance with different grid systems

Cases	Coarse Grid	Fine Grid
Number of cells	11184	44736
Flow rate at exit (kg/s)	0.123	0.122
Maximum static pressure (Pa)	373	375

5. RESULTS AND DISCUSSION

5.1 Baseline case: Existing Design

The computed pressure and temperature fields of the existing design are shown in Fig. 3, and the velocity field and stream function distribution are shown in Fig. 4.

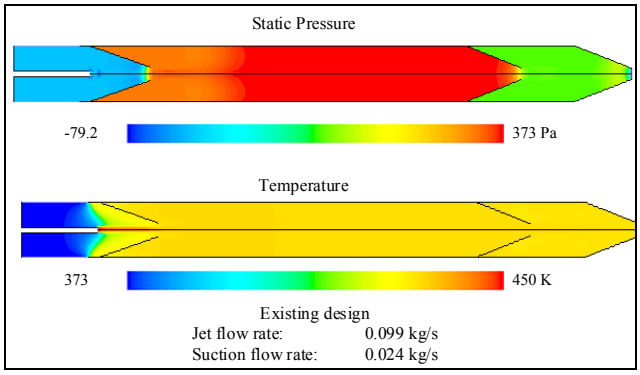

Figure 3: Pressure and temperature fields of the existing design

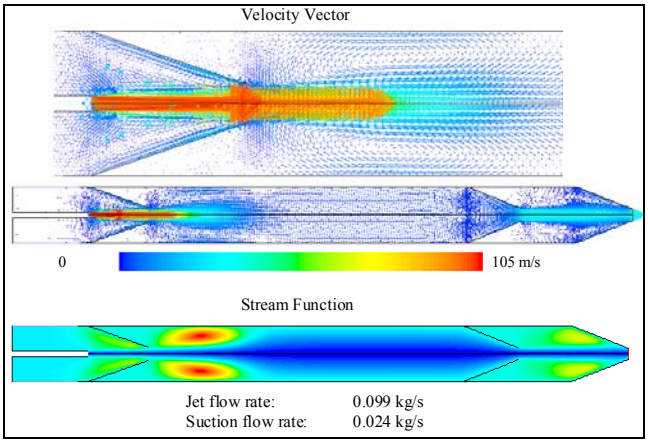

Figure 4: Velocity field and stream function of the existing design

The figures show the static pressure is high between the first and second contraction cones. The high temperature jet mixes with the cool entrained (sucked) steam to become a moderate temperature flow. Strong recirculation occurs inside the contraction cones and in the suddenly opened section immediately downstream of the contraction cones. The recirculation signifies inefficient aerodynamic performance and increased pressure losses as well as entropy production.

The simulation result indicates that the suction flow rate is only about 24% of the steam jet flow rate, which is significantly lower than the designed value of 350% of the jet flow rate. A suction rate can be defined as

$$\eta = \dot{m}_s / \dot{m}_j \tag{12}$$

It is essentially the ratio of mass flow rate of secondary (suction) flow and the jet flow. The low suction rate is considered as the main culprit of the low output of distilled water. Therefore, it is necessary to explore parameters that can potentially affect the suction flow rate. Almost more than 20 cases have been simulated, and only the cases with favorable results are presented next.

5.2 Effect of Downstream Contraction Cones

The effect of downstream contraction cones is conducted by removing one of the downstream cones each time. Figure 5 shows that the suction rate is increased from 24% to 50% by removing one cone, and removing both the cones downstream can lift the suction rate to 140% -- a six-fold augmentation! The reverse flow inside the contraction is apparently weakened; however, the flow recirculation downstream of the contraction still occurs, and the area of recirculation becomes even larger after the cone is removed. With both downstream contraction cones being removed, the suction flow rate increases, and the temperature of the mixed flow becomes lower, as shown in Fig. 5(b).

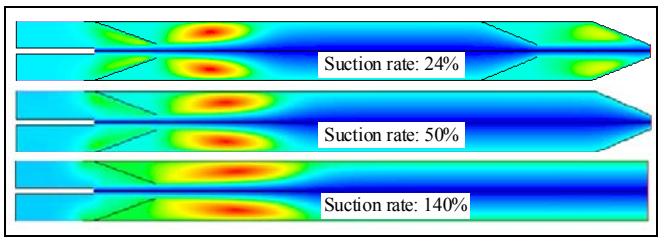

(a) Stream function

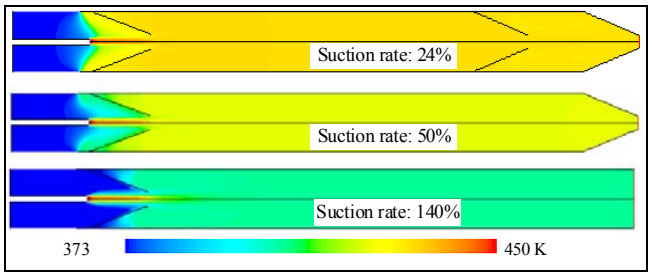

(b) Temperature

Figure 5: Effect of downstream resistance on the ejector flow pattern and suction rate

From these results, it can be clearly seen that the downstream contraction cones do not provide additional momentum transfer or suction power as originally designed. Instead, they adversely create high flow resistance and significantly impede the suction performance of the first-stage steam jet.

5.3 Effect of Adding a Downstream Diffuser

To reduce the flow recirculation downstream the contraction cone, a diffuser is added into the pipe following the design concept of the standard Venturi nozzle. The length of the diffuser is 1.68 m (66 inches), which gives a diffusing angle of 6.5^o to avoid flow separation near the wall. Figure 6 shows the comparison between the cases with and without the downstream diffuser. The flow recirculation area is oblivious in the downstream of the diffuser. The flow separation is negligible inside the diffuser. As a result, the suction rate is increased to 365%, a 2.6-fold increase from the case without the diffuser and 15.2 times more than the existing design. The temperature of mixed flow becomes even lower due to the high suction flow rate. Based on these results, it can be concluded that employing a downstream diffuser to reduce aerodynamic losses is extremely important. It is not difficult to completely remove the flow separation by reducing the diffuser's included angle to below 6^o, which will make the diffuser even longer.

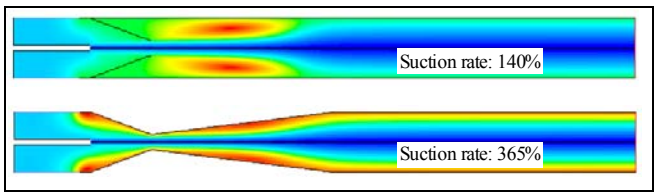

(a) Stream function

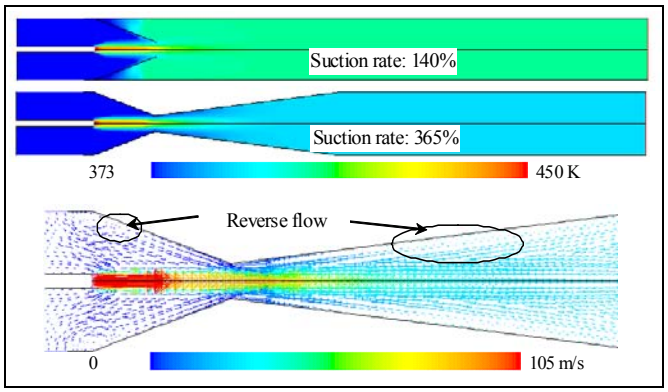

(b) Temperature and velocity vector

Figure 6: Effect of downstream diffuser on the ejector flow pattern and suction rate

5.4 Effect of the Location of the Steam Jet

To search for a more effective suction, the effect of the location of the steam jet exit is examined. Several cases are studied by moving the steam injecting location from at the contraction cone entrance away and into the contraction progressively. Figure 7 shows the results of the two cases: one is with the steam jet located in the plane of cone entrance, and the other case is with the steam jet being moved half way into the contraction cone. Both cases include one downstream contraction cone. It is seen that the reverse flow becomes stronger in the second case, which results in a reduction of suction flow rate from 50% to 18%. After comparing this with many other cases, it is concluded that the best result occurs by placing the steam jet injection right at the centerline at the contraction cone's entrance. A slight displacement of the jet will not result in any significant change in the suction flow rate.

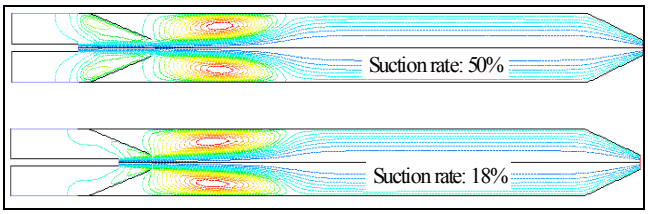

(a) Stream function

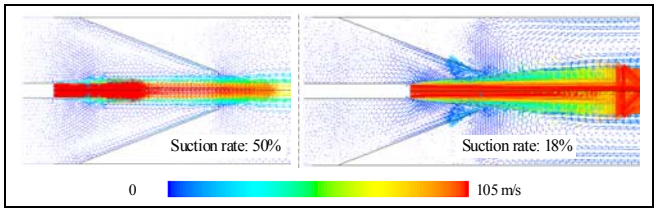

(b) Velocity vector

Figure 7: Effect of jet location on the flow field and ejector performance

5.5 Effect of the Contraction Cone Wall Contour

While the simple straight-wall contraction cone and diffuser are easier to manufacture than the contoured ones, the potential enhancement of the suction flow rate is investigated by adding contoured wall to the contraction cone. Figure 8 shows the results with a modified cone and diffuser geometry. The contraction cone has a contoured wall, and a small section of straight transition (4 inches) is added between the cone and diffuser to make the transition from the convergent cone to the divergent cone more smoothly. The result indicates the contoured contraction cone and the added transition piece indeed increase the suction rate about 20% from 365% to 430%. Note that due to the high suction flow, the maximum velocity is higher than the jet velocity in this case.

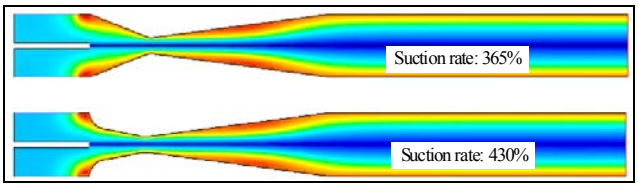

(a) Stream function

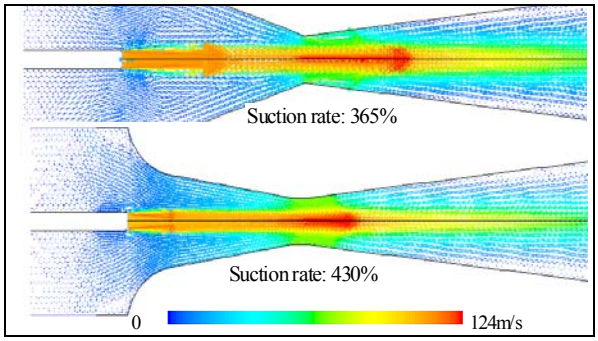

(b) Velocity vector

Figure 8: Effect of the contraction cone contour on the ejector performance

5.6 Effect of the Suction Opening Size

The suction opening is the section connecting the evaporating volume to the thermal ejector. The opening is initially designed into a cut-through section on the chamber wall housing the steam injector and the contraction cone. The opening is 0.61-m (24 inch) long and cut-through about one half of the pipe surface. As an approximation, the suction opening is treated as an axisymmetric opening slot during the simulation. Since it is not clear if the opening size would affect the suction flow rate, the effect of the suction opening size is examined. Two cases are compared: Case (a) has a baseline opening size, and Case (b) has a smaller suction opening (1/3 of the baseline opening). The results in Fig. 9 indicate that the stream function as well as the velocity vector does not change much in these two cases. The corresponding suction flow rates are almost the same at 365%.

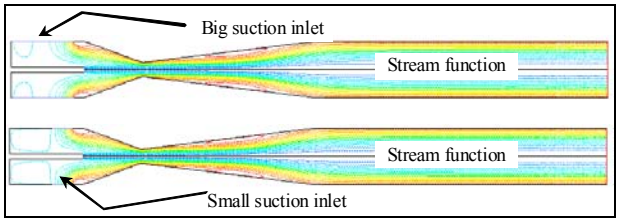

(a) Stream function

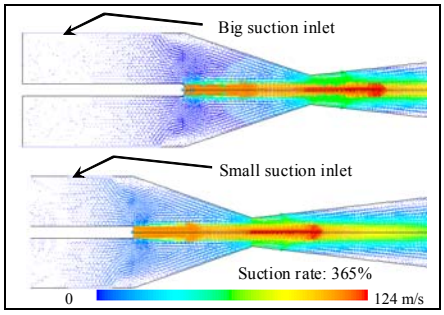

(b) Velocity vector

Figure 9: Effect of the suction opening size

5.7 Effect of Adding a Suction Flow Guide

Considering the large flow recirculation near the contraction entrance, a contoured flow guide is added between the existing contraction wall and the steam jet injection tube. Two cases are compared: one without and the other with the flow guide. Both cases have the downstream diffuser and a downstream contraction cone. The results in Fig. 10 show that these two cases have similar suction rate: 104% (0.103 kg/s) in the first case versus 99% (0.0982 kg/s) in the second. It can be seen that the benefit of adding the flow guide is negligible and is not worth the trouble of being added.

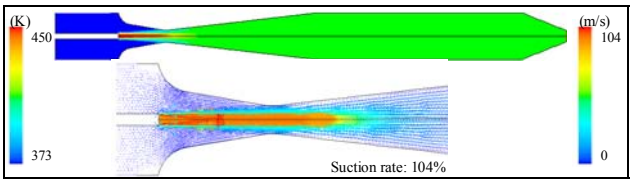

(a) Temperature and velocity without suction flow guide

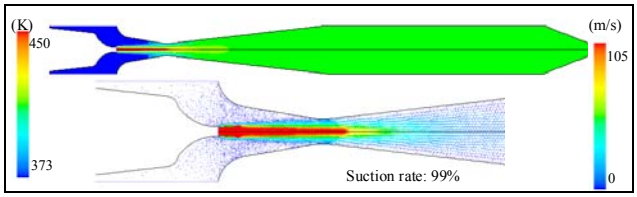

(b) Temperature and velocity vector with suction flow guide

Figure 10: Comparison of the ejector performance with and without suction flow guide

5.8 The Optimal Case

By combining all the favorable features together, an optimal case is simulated with a contoured contraction cone, a long diffuser downstream, a transition piece added between the contraction and the diffuser, and all downstream contraction cones removed. The result in Fig. 11 shows the smooth flow field with a minimized flow recirculation zone. The suction flow rate is 0.4233 kg/s or 430% the jet flow rate. Figure 12 compares the distributions of pressure and temperature along the ejector centerline between the optimal case and existing design. A significant deference can be clearly seen. Further optimization can be conducted.

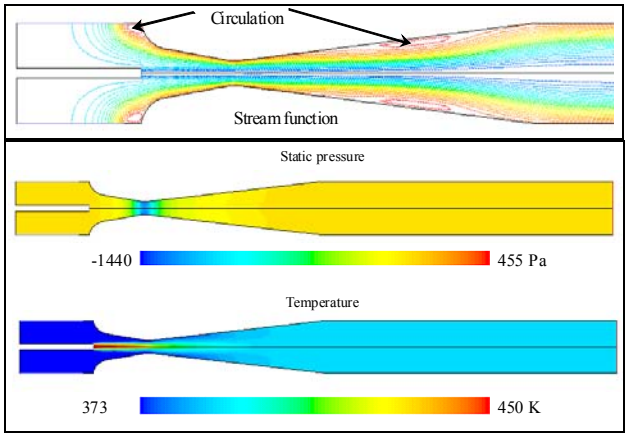

Figure 11: Flow pattern and temperature distribution for the optimized ejector case

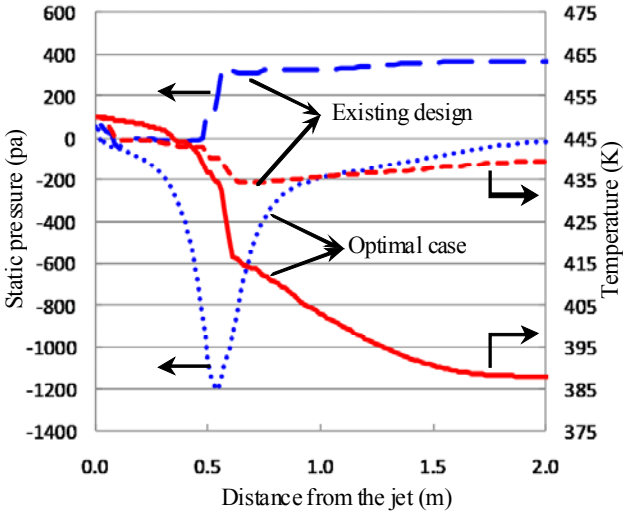

Figure 12: Temperature and pressure distributions along the ejector centerline in different cases

This study shows different ways to enhance the suction flow rate of the thermal compressor in a new steam evaporator. The actual suction flow rate is subject to the numerical uncertainty when applied to real situations; however, the concepts obtained from the numerical simulation are extremely useful and instrumental in providing the solution to the problems encountered by the existing system.

6. CONCLUSIONS

Based on numerical simulation, the following conclusions can be made:

1. The downstream contraction cones create large flow resistance and impede the overall suction performance. Neither additional momentum nor additional suction flow rate is provided as claimed in the existing design. Removing the downstream cones significantly increases the suction capacity. For example, the suction rate is doubled by removing the first contraction cone and increases 5.8 times by removing the second one.

2. Adding a diffuser downstream the contraction cone also provides a significant increase of the suction flow rate. A simple straight diffuser with an included angle of 6.5^{o} increases suction flow rate by 2.6 times.

3. The location of the steam jet exit affects the flow suction rate. The best location is at the center of the contraction cone entrance. The suction capacity reduces when the steam jet injection location is moved into or away from the entrance plane. When the injection location is placed half way between the entrance and the contraction exit, the suction capacity loses 67%.

4. Employing an aerodynamically contoured contraction cone provides a 20% augmentation of suction flow rate, which is definitely a favorable effect although not significant.

5. The suction opening connected to the vapor plenum is not important. Shrinking the suction opening to one or two-thirds of the original size does not change the suction flow rate.

6. Adding a contoured annular passage to guide the entrained flow shows little effect on the suction rate.

7. The optimal design is found by modifying the contraction cone wall profile to become aerodynamically contoured, adding a long diffuser downstream the contraction cone, removing all the contraction cones downstream, and locating the steam jet injection at the center of the contraction cone entrance. The suction rate of the optimal case is 0.423 kg/s, which is 4.3 times the flow rate of the steam jet and 18 times higher than the existing design.

REFERENCES

[1] Power, R.B., 1994, Steam jet ejectors for the process industries, McGraw-Hill, New York, NY, USA.

[2] Balamurugan, S., Gaikar, V.G., and Patwardhan, A.W., 2008, "Effect of ejector configuration on hydrodynamic characteristics of gas-liquid ejectors," Chemical Engineering Science, v. 63, pp. 721-731.

[3] Chen, Y.M., Sun, C. Y., 1997, "Experimental study of the performance characteristics of a steam-ejector refrigeration system," Experimental Thermal and Fluid Science, v.15, pp. 384-394.

[4] Rusly, E., Aye, Lu, Charters, W.W.S., and Ooi, A., 2005, "CFD analysis of ejector in a combined ejector cooling system," International Journal of Refrigeration, v. 28, pp. 1092-1101.

[5] Pianthong, K., Seehanam, W., Behnia, M., Sriveerakul, T., and Aphornratana, S., 2007, "Investigation and improvement of ejector refrigeration system using computational fluid dynamics technique," Energy Conversion and Management, v. 48, pp. 2556-2564.

[6] Riffat, S.B. and Everitt, P., 1999, "Experimental and CFD modelling of an ejector system for vehicle air conditioning," Journal of the Institute of Energy, v. 72, pp. 41-47.

[7] Ji, J., Ni, H., Li, L., Wang, R., 2008, "Performance simulation and analysis of steam ejector under different operating condition," Journal of Chemical Industry and Engineering (China), v. 59, pp. 557-561.

[8] Elkady, M., Karameldin, A., Negeed, E.S., and El-Bayoumy, R, 2008, "Experimental investigation of the effect of ejector geometry on its performance," International Journal of Nuclear Desalination, v. 3, pp. 215-229.

[9] Negeed, E-S. R., 2009, "Enhancement of ejector performance for a desalination system," International Journal of Nuclear Desalination, v. 3, pp.247-259.

[10] Kim, H.D., Lee, J.H., Setoguchi, T., and Matsuo, S., 2006, "Computational analysis of a variable ejector flow," Journal of Thermal Science, v. 15, pp. 140-144.

[11] Kim, H.D., Lee, J.H., Setoguchi, T., and Matsuo, S., 2006, "Optimization study of a Coanda ejector," Journal of Thermal Science, v. 15, pp. 331-336.

[12] Sriveerakul, T., Aphornratana, S., Chunnanond, K., 2007, "Performance prediction of steam ejector using computational fluid dynamics: Part 2. Flow structure of a steam ejector influenced by operating pressures and

geometries," Int. J. of Thermal Sciences, v. 46, pp. 823-833.
[13] Choudhury, D., 1993, "Introduction to the Renormalization Group Method and Turbulence Modeling," Fluent Inc. Technical Memorandum TM-107.
[14] Wolfstein, M., 1969, "The Velocity and Temperature Distribution of One-Dimensional Flow with Turbulence Augmentation and Pressure Gradient," Int. J. Heat Mass Transfer, v. 12**,** pp. 301-318.
[15] Fluent Manual, Version 6.3.23, Fluent Inc, 2006.
[16] Patankar, S.V., Numerical Heat Transfer and Fluid Flow, McGraw-Hill, New York, USA, 1980.